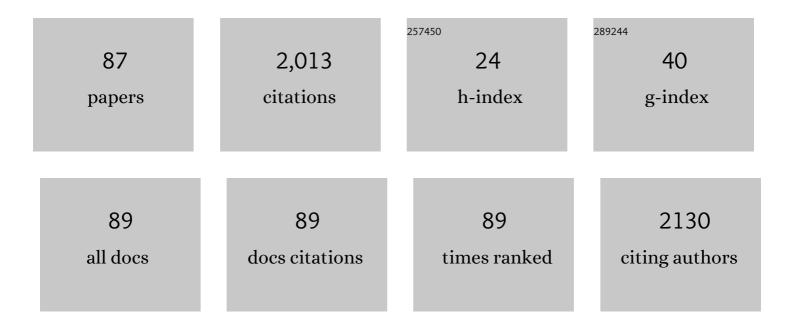
Chao Liu

List of Publications by Year in descending order

Source: https://exaly.com/author-pdf/980768/publications.pdf Version: 2024-02-01



#	Article	IF	CITATIONS
1	The absorption Ãngström exponent of black carbon: from numerical aspects. Atmospheric Chemistry and Physics, 2018, 18, 6259-6273.	4.9	158
2	On the radiative properties of ice clouds: Light scattering, remote sensing, and radiation parameterization. Advances in Atmospheric Sciences, 2015, 32, 32-63.	4.3	141
3	An unexpected catalyst dominates formation and radiative forcing of regional haze. Proceedings of the United States of America, 2020, 117, 3960-3966.	7.1	132
4	Estimating Summertime Precipitation from Himawari-8 and Global Forecast System Based on Machine Learning. IEEE Transactions on Geoscience and Remote Sensing, 2019, 57, 2557-2570.	6.3	91
5	Application of the pseudo-spectral time domain method to compute particle single-scattering properties for size parameters up to 200. Journal of Quantitative Spectroscopy and Radiative Transfer, 2012, 113, 1728-1740.	2.3	76
6	Numerical investigation on the Ångström exponent of black carbon aerosol. Journal of Geophysical Research D: Atmospheres, 2016, 121, 3506-3518.	3.3	53
7	Comparison between the pseudo-spectral time domain method and the discrete dipole approximation for light scattering simulations. Optics Express, 2012, 20, 16763.	3.4	49
8	Numerical accuracy of "equivalent―spherical approximations for computing ensemble-averaged scattering properties of fractal soot aggregates. Journal of Quantitative Spectroscopy and Radiative Transfer, 2010, 111, 2127-2132.	2.3	48
9	The Influence of Water Coating on the Optical Scattering Properties of Fractal Soot Aggregates. Aerosol Science and Technology, 2012, 46, 31-43.	3.1	46
10	Optical properties of black carbon aggregates with non-absorptive coating. Journal of Quantitative Spectroscopy and Radiative Transfer, 2017, 187, 443-452.	2.3	45
11	Inhomogeneity structure and the applicability of effective medium approximations in calculating light scattering by inhomogeneous particles. Journal of Quantitative Spectroscopy and Radiative Transfer, 2014, 146, 331-348.	2.3	42
12	The Effects of Monomer Size Distribution on the Radiative Properties of Black Carbon Aggregates. Aerosol Science and Technology, 2015, 49, 928-940.	3.1	42
13	Modulations of surface thermal environment and agricultural activity on intraseasonal variations of summer diurnal temperature range in the Yangtze River Delta of China. Science of the Total Environment, 2020, 736, 139445.	8.0	39
14	Seasonal variation of columnar aerosol optical properties and radiative forcing over Beijing, China. Atmospheric Environment, 2017, 166, 340-350.	4.1	38
15	Comparison of Cloud Properties from Himawari-8 and FengYun-4A Geostationary Satellite Radiometers with MODIS Cloud Retrievals. Remote Sensing, 2019, 11, 1703.	4.0	38
16	Additional global climate cooling by clouds due to ice crystal complexity. Atmospheric Chemistry and Physics, 2018, 18, 15767-15781.	4.9	37
17	A highly agricultural river network in Jurong Reservoir watershed as significant CO2 and CH4 sources. Science of the Total Environment, 2021, 769, 144558.	8.0	35
18	Black carbon aggregates: A database for optical properties. Journal of Quantitative Spectroscopy and Radiative Transfer, 2019, 222-223, 170-179.	2.3	34

#	Article	IF	CITATIONS
19	Basin-wide responses of the South China Sea environment to Super Typhoon Mangkhut (2018). Science of the Total Environment, 2020, 731, 139093.	8.0	34
20	Global Distribution of Three Types of Drop Size Distribution Representing Heavy Rainfall From GPM/DPR Measurements. Geophysical Research Letters, 2021, 48, e2020GL090871.	4.0	32
21	The colors of biomass burning aerosols in the atmosphere. Scientific Reports, 2016, 6, 28267.	3.3	28
22	Optical Properties and Radiative Forcing of Aged BC due to Hygroscopic Growth: Effects of the Aggregate Structure. Journal of Geophysical Research D: Atmospheres, 2019, 124, 4620-4633.	3.3	27
23	A fast Visible Infrared Imaging Radiometer Suite simulator for cloudy atmospheres. Journal of Geophysical Research D: Atmospheres, 2015, 120, 240-255.	3.3	26
24	Atmospheric heating rate due to black carbon aerosols: Uncertainties and impact factors. Atmospheric Research, 2020, 240, 104891.	4.1	26
25	Pacific Meridional Modeâ€Western North Pacific Tropical Cyclone Linkage Explained by Tropical Pacific Quasiâ€Decadal Variability. Geophysical Research Letters, 2019, 46, 13346-13354.	4.0	24
26	Accounting for the effects of nonideal minor structures on the optical properties of black carbon aerosols. Atmospheric Chemistry and Physics, 2019, 19, 2917-2931.	4.9	24
27	Same Initial States Attack in Yang et al.'s Quantum Private Comparison Protocol and the Improvement. International Journal of Theoretical Physics, 2014, 53, 271-276.	1.2	22
28	A multilayer cloud detection algorithm for the Suomi-NPP Visible Infrared Imager Radiometer Suite (VIIRS). Remote Sensing of Environment, 2019, 227, 1-11.	11.0	22
29	Secure Quantum Private Comparison of Equality Based on Asymmetric W State. International Journal of Theoretical Physics, 2014, 53, 1804-1813.	1.2	21
30	Can atmospheric reanalyses (CRA and ERA5) represent cloud spatiotemporal characteristics?. Atmospheric Research, 2020, 244, 105091.	4.1	21
31	Evaluation of cloud properties from reanalyses over East Asia with a radiance-based approach. Atmospheric Measurement Techniques, 2020, 13, 1033-1049.	3.1	21
32	A Machine Learning-based Cloud Detection Algorithm for the Himawari-8 Spectral Image. Advances in Atmospheric Sciences, 2022, 39, 1994-2007.	4.3	21
33	ENSO Regime Changes Responsible for Decadal Phase Relationship Variations Between ENSO Sea Surface Temperature and Warm Water Volume. Geophysical Research Letters, 2019, 46, 7546-7553.	4.0	20
34	Leveraging machine learning for quantitative precipitation estimation from Fengyun-4 geostationary observations and ground meteorological measurements. Atmospheric Measurement Techniques, 2021, 14, 7007-7023.	3.1	20
35	Performance of the discrete dipole approximation for optical properties of black carbon aggregates. Journal of Quantitative Spectroscopy and Radiative Transfer, 2018, 221, 98-109.	2.3	19
36	Diurnal haze variations over the North China plain using measurements from Himawari-8/AHI. Atmospheric Environment, 2019, 210, 100-109.	4.1	19

#	Article	IF	CITATIONS
37	Different Effects of Two ENSO Types on Arctic Surface Temperature in Boreal Winter. Journal of Climate, 2019, 32, 4943-4961.	3.2	18
38	Review of Chinese atmospheric science research over the past 70 years: Atmospheric physics and atmospheric environment. Science China Earth Sciences, 2019, 62, 1903-1945.	5.2	18
39	The process of methanogenesis in paddy fields under different elevated CO2 concentrations. Science of the Total Environment, 2021, 773, 145629.	8.0	18
40	High-Spatial-Resolution Population Exposure to PM2.5 Pollution Based on Multi-Satellite Retrievals: A Case Study of Seasonal Variation in the Yangtze River Delta, China in 2013. Remote Sensing, 2019, 11, 2724.	4.0	17
41	Estimation of radiative forcing and heating rate based on vertical observation of black carbon in Nanjing, China. Science of the Total Environment, 2021, 756, 144135.	8.0	17
42	Improved Deterministic N-To-One Joint Remote Preparation of an Arbitrary Qubit via EPR Pairs. International Journal of Theoretical Physics, 2015, 54, 472-483.	1.2	16
43	Effects and Applications of Satellite Radiometer 2.25- <inline-formula> <tex-math notation="LaTeX">\$mu\$ </tex-math </inline-formula> m Channel on Cloud Property Retrievals. IEEE Transactions on Geoscience and Remote Sensing, 2018, 56, 5207-5216.	6.3	16
44	An investigation of the implications of lunar illumination spectral changes for Day/Night Bandâ€based cloud property retrieval due to lunar phase transition. Journal of Geophysical Research D: Atmospheres, 2017, 122, 9233-9244.	3.3	14
45	Retrieval of cloud properties from thermal infrared radiometry using convolutional neural network. Remote Sensing of Environment, 2022, 278, 113079.	11.0	14
46	A closure study of aerosol optical properties at a regional background mountainous site in Eastern China. Science of the Total Environment, 2016, 550, 950-960.	8.0	13
47	Modulation of tropical cyclones in the southeastern part of western North Pacific by tropical Pacific decadal variability. Climate Dynamics, 2019, 53, 4475-4488.	3.8	13
48	Application of machine learning to hyperspectral radiative transfer simulations. Journal of Quantitative Spectroscopy and Radiative Transfer, 2020, 246, 106928.	2.3	13
49	Spatiotemporal characteristics and risk assessment of agricultural drought disasters during the winter wheat-growing season on the Huang-Huai-Hai Plain, China. Theoretical and Applied Climatology, 2021, 143, 1393-1407.	2.8	13
50	Can light absorption of black carbon still be enhanced by mixing with absorbing materials?. Atmospheric Environment, 2021, 253, 118358.	4.1	13
51	Retrieval of Iceâ€Overâ€Water Cloud Microphysical and Optical Properties Using Passive Radiometers. Geophysical Research Letters, 2020, 47, e2020GL088941.	4.0	12
52	Scattering matrices of mineral dust aerosols: aÂrefinement of the refractive index impact. Atmospheric Chemistry and Physics, 2020, 20, 2865-2876.	4.9	12
53	Radianceâ€Based Evaluation of WRF Cloud Properties Over East Asia: Direct Comparison With FYâ€2E Observations. Journal of Geophysical Research D: Atmospheres, 2018, 123, 4613-4629.	3.3	11
54	Reproducing the morphology-dependent resonances of spheres with the discrete dipole approximation. Optics Express, 2019, 27, 22827.	3.4	11

#	Article	IF	CITATIONS
55	Assessing the Accuracy of Forest Phenological Extraction from Sentinel-1 C-Band Backscatter Measurements in Deciduous and Coniferous Forests. Remote Sensing, 2022, 14, 674.	4.0	10
56	Recent Progress in Impacts of Mixing State on Optical Properties of Black Carbon Aerosol. Current Pollution Reports, 2020, 6, 380-398.	6.6	9
57	A Spectral Data Compression (SDCOMP) Radiative Transfer Model for High-Spectral-Resolution Radiation Simulations. Journals of the Atmospheric Sciences, 2020, 77, 2055-2066.	1.7	9
58	Effects of elevated carbon dioxide on metal transport in soil-crop system: results from a field rice and wheat experiment. Journal of Soils and Sediments, 2019, 19, 3742-3748.	3.0	8
59	Study of Terrestrial Clints Based on DSCOVR Observations. Earth and Space Science, 2019, 6, 166-173.	2.6	8
60	Recordâ€Low WNP Tropical Cyclone Activity in Early Summer 2020 due to Indian Ocean Warming and Maddenâ€Julian Oscillation Activity. Geophysical Research Letters, 2021, 48, e2021GL094578.	4.0	8
61	Methane emissions in japonica rice paddy fields under different elevated CO2 concentrations. Nutrient Cycling in Agroecosystems, 2022, 122, 173-189.	2.2	8
62	Extreme Indian Ocean dipole events associated with El Niño and Madden–Julian oscillation. Climate Dynamics, 2022, 59, 1953-1968.	3.8	8
63	Combination of AIRS Dual CO2 Absorption Bands to Develop an Ice Clouds Detection Algorithm in Different Atmospheric Layers. Remote Sensing, 2020, 12, 6.	4.0	7
64	A robust relationship between multidecadal global warming rate variations and the Atlantic Multidecadal Variability. Climate Dynamics, 2020, 55, 1945-1959.	3.8	7
65	An accurate and efficient radiative transfer model for simulating all-sky images from Fengyun satellite radiometers. Science China Earth Sciences, 2020, 63, 1701-1713.	5.2	7
66	Responses of CO2 and N2O emissions from soil-plant systems to simulated warming and acid rain in cropland. Journal of Soils and Sediments, 2021, 21, 1109-1126.	3.0	7
67	Significant Contribution of Coarse Black Carbon Particles to Light Absorption in North China Plain. Environmental Science and Technology Letters, 2022, 9, 134-139.	8.7	7
68	Implementation of a 1â€Ð Thermodynamic Model for Simulating the Winterâ€Time Evolvement of Physical Properties of Snow and Ice Over the Arctic Ocean. Journal of Advances in Modeling Earth Systems, 2021, 13, e2020MS002448.	3.8	6
69	A method to dynamically constrain black carbon aerosol sources with online monitored potassium. Npj Climate and Atmospheric Science, 2021, 4, .	6.8	6
70	Detecting Multilayer Clouds From the Geostationary Advanced Himawari Imager Using Machine Learning Techniques. IEEE Transactions on Geoscience and Remote Sensing, 2022, 60, 1-12.	6.3	6
71	Numerical simulation of raindrop scattering for C-band dual-polarization Doppler weather radar parameters. Journal of Quantitative Spectroscopy and Radiative Transfer, 2018, 213, 133-142.	2.3	5
72	Spatiotemporal distributions of cloud radiative forcing and response to cloud parameters over the Mongolian Plateau during 2003–2017. International Journal of Climatology, 2020, 40, 4082-4101.	3.5	5

#	Article	IF	CITATIONS
73	Hyperspectral characteristics and inversion model estimation of winter wheat under different elevated CO2 concentrations. International Journal of Remote Sensing, 2021, 42, 1035-1053.	2.9	5
74	A bimodal distribution of haze in Pluto's atmosphere. Nature Communications, 2022, 13, 240.	12.8	5
75	Long-term multidataset direct aerosol radiative forcing and its efficiencies: Intercomparisons and uncertainties. Atmospheric Research, 2022, 267, 105964.	4.1	5
76	Equatorial Origin of the Observed Tropical Pacific Quasiâ€Đecadal Variability From ENSO Nonlinearity. Geophysical Research Letters, 2022, 49, .	4.0	5
77	Optical Properties of Black Carbon Aggregates. Springer Series in Light Scattering, 2019, , 167-218.	0.6	4
78	Distinctive MJO Activity during the Boreal Winter of the 2015/16 Super El Niño in Comparison with Other Super El Niño Events. Advances in Atmospheric Sciences, 2021, 38, 555-568.	4.3	4
79	Effects of Linear Calibration Errors at Low-Temperature End of Thermal Infrared Band: Lesson From Failures in Cloud Top Property Retrieval of FengYun-4A Geostationary Satellite. IEEE Transactions on Geoscience and Remote Sensing, 2022, 60, 1-11.	6.3	4
80	Assessing Overlapping Cloud Top Heights: An Extrapolation Method and Its Performance. IEEE Transactions on Geoscience and Remote Sensing, 2022, 60, 1-11.	6.3	4
81	Characteristics and influencing factors of carbon fluxes in winter wheat fields under elevated CO2 concentration. Environmental Pollution, 2022, 307, 119480.	7.5	4
82	Information Content of Ice Cloud Properties from Multi-Spectral, -Angle and -Polarization Observations. Remote Sensing, 2020, 12, 2548.	4.0	3
83	Detecting supercooled water clouds using passive radiometer measurements. Geophysical Research Letters, 0, , .	4.0	3
84	Can the Aerosol Absorption Ãngström Exponent Represent Aerosol Color in the Atmosphere: A Numerical Study. Atmosphere, 2020, 11, 187.	2.3	2
85	Hyperspectral characteristics and leaf area index monitoring of rice (Oryza sativa L.) under carbon dioxide concentration enrichment. Spectroscopy Letters, 2021, 54, 231-243.	1.0	2
86	Characterizing unforced decadal climate variability in global climate model large ensembles. Climate Dynamics, 2022, 58, 211-222.	3.8	2
87	High-resolution typhoon precipitation integrations using satellite infrared observations and multisource data. Atmospheric Measurement Techniques, 2022, 15, 2791-2805.	3.1	0